Journal of Drug Delivery Science and Technology 117 (2026) 107986

Contents lists available at ScienceDirect

Journal of Drug Delivery Science and Technology

journal homepage: www.elsevier.com/locate/jddst

Dual release of miRNA-424-3p and doxorubicin using layer-by-layer stimuli-responsive dendritic mesoporous nanoparticles

Oznur Akbal Vural [a,b,*], Tayfun Vural [a], Vicente Martí-Centelles [a,c,f], Estela Climent [a,c,e], Alba García-Fernández [a,c,d], Ramón Martínez-Máñez [a,c,d,e,f,**]

[a] Instituto Interuniversitario de Investigación de Reconocimiento Molecular y Desarrollo Tecnológico (IDM), Universitat Politècnica de València, Universitat de València, Camino de Vera s/n, 46022, Valencia, Spain
[b] Advanced Technologies Application and Research Center, Hacettepe University, Beytepe Campus, Cankaya, 06800, Ankara, Turkiye
[c] CIBER de Bioingeniería Biomateriales y Nanomedicina (CIBER-BBN), Instituto de Salud Carlos III, 28029, Madrid, Spain
[d] Unidad Mixta UPV-CIPF de Investigación en Mecanismos de Enfermedades y Nanomedicina, Valencia, Universitat Politècnica de València, Centro de Investigación Príncipe Felipe, Avenida Eduardo Primo Yúfera, 3, 46012, Valencia, Spain
[e] Unidad Mixta de Investigación en Nanomedicina y Sensores, Universitat Politècnica de València, Instituto de Investigación Sanitaria La Fe (IIS La Fe), Avenida Fernando Abril Martorell, 106, 46026, Valencia, Spain
[f] Departamento de Química, Universitat Politècnica de València, Camino de Vera s/n, 46022, Valencia, Spain

ARTICLE INFO

Keywords:
miRNA-424-3p
Doxorubicin
Dendritic mesoporous silica nanoparticles
Galectin-3
Gene therapy

ABSTRACT

The prevalence of cancer is on the rise on a global scale, and lung cancer represents one of the most common types of cancer worldwide that leads to high cancer-related deaths. Over the past decade, nanotechnology has made tremendous progress in cancer treatment. Moreover, combination therapy, including chemotherapy and gene therapy, has turned out to be a promising strategy that could enhance therapeutic efficacy in the treatment of lung adenocarcinoma. The tumor-suppressive miRNA-424-3p has demonstrated to significantly downregulate galectin-3 (Gal3) which is an anti-apoptotic protein and highly expressed in A549 cells. This has been shown to promote apoptosis, decrease proliferation, and increase sensitivity to the chemotherapeutic drug doxorubicin (Dox). However, miRNA-424-3p-based combination therapies with Dox have not yet been reported. Since dendritic mesoporous silica nanoparticles (DMSNs) have the potential to act as carriers for nucleic acids and drugs simultaneously, in this study we have successfully introduced for the first time anti-Gal3 functionalized DMSNs for the co-delivery of miRNA-424-3p and Dox protected with a layer-by-layer polyethyleneimine and poly-L-lysine coating. Whereas there is no or minimal Dox and miRNA release under neutral pH from the nanoparticles, conversely, a significant delivery of Dox and miRNA is seen in lysosomal extract medium. The effects of the co-delivery system, i.e. miRNA-424-3p and Dox, on A549 cells is evaluated by analyzing cell proliferation, cellular uptake, cell apoptosis assay, and the expression of related proteins and genes. The results demonstrate that miRNA-424-3p effectively transfected into A549 lung cancer cells, dramatically reducing the expression of Gal3 at the protein level. Forward transfection of the cell line with the DMSN loaded with miRNA-424-3p and Dox causes both a decrease in cell viability and an increase in apoptosis induction. Our data shows that the designed DMSN has a good performance as a combined drug and gene delivery system for cancer therapy.

1. Introduction

The burden of cancer incidence and mortality is growing fast worldwide, being lung cancer one of the most common types of cancer. With the help of improvements in therapeutic strategies, such as surgery, chemotherapy, radiotherapy and immunotherapy, the prognosis of lung cancer has gradually advanced [1,2]. However, the recurrence rate of lung cancer is 10–60 % after surgery [3]. Thus, to enhance patient

* Corresponding author. Instituto Interuniversitario de Investigación de Reconocimiento Molecular y Desarrollo Tecnológico (IDM), Universitat Politècnica de València, Universitat de València, Camino de Vera s/n, 46022, Valencia, Spain
** Corresponding author. Instituto Interuniversitario de Investigación de Reconocimiento Molecular y Desarrollo Tecnológico (IDM), Universitat Politècnica de València, Universitat de València, Camino de Vera s/n, 46022, Valencia, Spain
E-mail addresses: oznurakbal@hacettepe.edu.tr (O.A. Vural), rmaez@qim.upv.es (R. Martínez-Máñez).

https://doi.org/10.1016/j.jddst.2026.107986
Received 14 July 2025; Received in revised form 1 December 2025; Accepted 5 January 2026
Available online 5 January 2026
1773-2247/© 2026 The Authors. Published by Elsevier B.V. This is an open access article under the CC BY-NC license (http://creativecommons.org/licenses/by-nc/4.0/).

outcomes, new therapeutic approaches are required. In this scenario, nanomaterials-based targeted delivery and controlled drug release are essential in personalized therapy. On that sense, mesoporous silica nanoparticles (MSNs) serve as advanced controlled drug release systems with stimulus-responsive properties [4–7]. Among MSNs, dendritic MSNs (DMSNs) with small particle size and center-radial pores are excellent candidates to attain high loading capacities and easy cellular absorption, increasing the delivery efficiency [8,9]. DMSNs are suitable for biological applications due to their higher surface area compared to classical MSNs [10]. DMSNs allow the encapsulation of large payloads like enzymes, DNA, etc. [11,12], and grafting of active molecules on the surface [10]. DMSNs have been engineered to induce cancer cell death and regression of solid tumors [13].

The interaction or communication of cancer cells within the tumor microenvironment decisively modulates cancer progression. On that regard, galectin-3 (Gal3, an anti-apoptotic protein coded by the LGALS3 gene) has attracted significant interest in cancer research due to its function in cancer progression and metastasis [14]. Gal3 is an intra-extracellular protein and has high expression levels in lung cancers when compared with healthy individuals [14–16]. It promotes chemo-resistance in lung cancer via binding β-galactosidases and is assumed as a lung cancer biomarker [17,18]. Several preclinical studies have shown that preventing Gal3 activity, either by blocking its gene expression or inhibiting its function, resulted in promising outcomes [19]. Hence, decreasing the level of Gal3 expression in a neoplasm may be a persuasive treatment method and this could be performed by using specific microRNAs (miRNAs). miRNAs have naturally evolved to control gene networks by interfering with transcripts that contain a partly complementary pattern on the mRNA's 3′ untranslated regions [20–22]. In this context, Ramasamy et al. found out that galectin-3 mRNA 3′UTR has the target sequence for miRNA-424-3p [23,24]. It has also been reported that miRNA-424-3p suppresses the expression of Gal3 [23,25]. DMSN is a potential carrier system for miRNA-424-3p as Gal3 suppressor to inhibit cancer development.

The combination of nucleic acid therapeutics such as miRNA with chemotherapy drugs such as Dox would be an effective way to achieve higher therapeutic efficiency. Dox, a potent chemotherapy drug, is a cytostatic agent in lung cancer chemotherapy [26]. miRNA therapeutics combined with chemotherapy drugs have the potential to enhance the efficacy of chemotherapy. The combination therapy with a carrier nanosystem reduces the risk of side effects caused by the cytotoxicity of chemotherapeutic drugs that are usually used alone as a first-line treatment for many cancers [27]. Besides, the knockdown of Gal3 with miRNA 424-3p as an effective inhibitor may decrease cancer cell growth and promote apoptosis. Therefore, the co-delivery of miRNA-424-3p and Dox using DMSN is expected to improve the therapeutic efficacy for lung cancer. As far as we know, this combination has not been previously reported.

In this study, we have developed an effective combination therapy nanosystem based on a DMSNs loaded with doxorubicin (Dox) and miR-424-3p. The nanosystem is formed by dendritic mesoporous silica nanoparticles containing Dox in the pores, which are protected using a layer-by-layer (LbL) strategy employing polyethylene imine (PEI) as a first layer followed by miRNA-424-3p as second layer and poly-L-lysine (PLL) as third layer, which is also covalently functionalized with an anti-Gal3 antibody as targeting agent (Scheme 1). This design primarily aims to obtain a dual effective nanoparticle system carrying a chemotherapy drug, Dox, and a gene silencing agent, miRNA-424-3p. In the nanosystem, PEI has dual function, acting as a delivery vehicle and as a gatekeeper allowing the release of Dox and miRNA-424-3p only in the acidic environment of lysosomes due to the protonation of PEI chains in acidic media. Moreover, PLL is a biocompatible molecule that reduces protein adsorption to the surface of nanoparticles and their immunogenicity [28], whereas the attachment of anti-Gal3 on the PLL layer would help to reach the tumor area. *In-vitro* drug release profiles are investigated in detail in phosphate-buffered saline solutions (PBS, pH 7.4) to simulate physiological conditions, and in lysosomal extract (pH 4.5–5.0) to mimic the acidic intracellular compartments responsible for stimulus-responsive cargo release. The Gal3-mediated endocytosis of the nanocarrier and the dual delivery of Dox and miRNA into A549 lung cancer cells is investigated by fluorescence monitoring and by cell viability, cell apoptosis, and Gal3 mRNA and protein analysis.

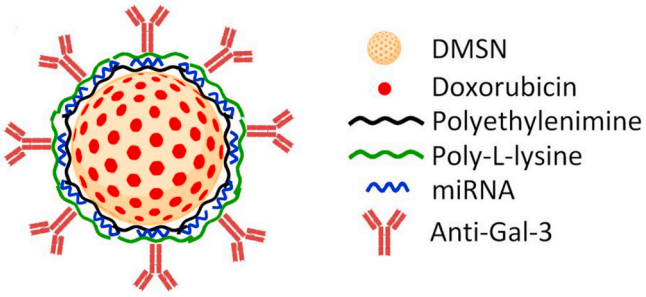

Scheme 1. Schematic representation of the **S7** delivery system.

2. Materials and methods

2.1. Reagents and chemicals

Tetraethyl orthosilicate (TEOS, 98 %), cetyltrimethylammonium bromide (CTABr, 95 %), polyethylenimine (PEI; average molecular weight: 25000 g/mol), poly-L-lysine (0.01 %), phosphate buffer solution (PBS, 10 mM, pH 7.4), Galectin-3 monoclonal antibody, N-hydroxysuccinimide (NHS), 1-[3-(dimethylamino]-propyl]-3-ethyl carbodiimide hydrochloride (EDC), doxorubicin, and lysosome Isolation Kit (LYSISO1) used for release studies was collected from Sigma Aldrich. (St. Louis, MO). Sodium perfluorooctanoate (FC8, ≥97 %) was purchased from Santa Cruz Biotechnology. Dulbecco's Modified Eagle's medium-high glucose (DMEM-HG), penicillin-streptomycin (10000 U/mL), and l-glutamine were purchased from Invitrogen (Carlsbad, CA). Fetal Bovine Serum (FBS) was from Atlanta Biologicals, Inc. (Lawrenceville, GA). Lipofectamine RNAi Max Transfection Reagent was collected from Thermo Fisher Scientific (Waltham, MA). Cell proliferation reagent WST-1 was purchased from Roche Diagnostics GmbH (Mannheim, Germany). Human Galectin-3 ELISA Kit and CoraLite® Plus 488-Annexin V and PI Apoptosis Kit were purchased from Proteintech (IL, USA). Pierce™ BCA Protein Assay Kit was purchased from Thermo Scientific (Rockford, USA). miRNeasy® Mini Kit for RNA isolation from Qiagen. PrimeScript RT Reagent Kit (Perfect Real Time) for cDNA synthesis was gathered from Takara Bio Inc. (Shiga, Japan). The hsa-miRNA-424-3p mimic with the sequence 5′-CAAAACGUGAGGCGCUGCUAU-3′ was purchased from Invitrogen (miRVana mimic assay ID MC12641, cat 4464066, Invitrogen). Doxorubicin was collected from Sigma-Aldrich. (St. Louis, MO). For all experiments and analyses, water was deionized, for miRNA preparation DNase-RNase free water was used (Thermo-Scientific). All chemicals were reagent grade and used without further purification or modification.

2.2. General technics and instrumentation

Transmission electron microscopy (TEM) images were recorded at 100 kV in a JEOL JEM-1010 microscope (JEOL Europe SAS, Croissysur-Seine, France), and TEM-energy dispersive X-ray (EDX) analysis was collected in a JEOL JEM-2100F (JEOL Europe SAS) working at 200 kV equipped with an X-ray detector. An amount of sample powder was dissolved in ethanol, and the mixture was sonicated for 15 min. A drop of the dispersed solution (5 μL) was carefully placed on a copper grid coated with carbon mesh and allowed to dry overnight. and SEM images were recorded using JEOL JSM 7800 field-emission scanning electron microscope (HRFESEM). For this, samples were suspended in water,

dropped to onto an SEM grid, and covered with conductive carbon film. X-ray diffraction (XRD) analysis was collected by a diffractometer using Cu-Kα radiation (D8 Advance, Philips Amsterdam, Netherlands) to examine the physical nature—whether crystalline or amorphous before and after calcination of DMSN. Porosity and surface properties of nanoparticles were recorded by N_2 adsorption-desorption isotherms measured with a Micromeritics ASAP 2010 automated desorption analyzer (Micromeritics Instrument Corporation, Norcross, GA, USA). Samples Lyophilized samples were degassed at 120 °C under a vacuum for overnight. Following a cooling period, the sample tube was transferred to the analysis port and immersed in a liquid nitrogen bath to ensure isothermal conditions were maintained. Pore size was determined by using the Barret-Joyner-Halenda (BJH) method. The specific surface areas were measured from the adsorption data in the low-pressure range using the Brunauer−Emmett−Teller (BET) model. Thermogravimetric analysis (TGA) was recorded by TGA/SDTA 851e (Mettler Toledo, Columbus, OH, USA) under an oxidant atmosphere (air, 80 mL/min) with a heating rate of 10 °C/min from 25 °C to 100 °C, an isothermal heating step at 100 °C for 60 min, a heating rate of 10 °C/min from 100 °C to 1000 °C. Dynamic light scattering (DLS) and ζ potential analysis were performed with a Malvern Zetasizer Nano ZS. For this, samples were diluted with distilled water (1 mg/mL). Measurements were conducted at a controlled temperature of 25 °C and a fixed detection angle of 90°. Each sample was analyzed in triplicate by using an instrument cuvette for size and a folded capillary zeta cell for zeta potential analysis. Fourier transform infrared (FTIR) analysis was collected on a Vertex 70 V FTIR spectrometer (Bruker, Billerica, Massachusetts) from 4000 to 500 cm^{-1} to identify potential chemical interactions or alterations in functional groups. The analysis includes DMSN, **S1**, **S6**, and ***S7***.

2.3. Synthesis of materials

Nanoparticles in this study were synthesized using a layer-by-layer assembly strategy. With each additional layer introduced after the synthesis process of DMSN, the resulting nanomaterial was assigned a new name ranging from S1 to S8. Moreover, control nanoparticles (**S3**) were synthesized by following the same procedure without the addition of Dox and miR-424-3p. The detailed synthesis procedures for these nanomaterials at each stage, from DMSN to S1 through S8, are described below.

2.3.1. Synthesis of dentritic mesoporous Silica nanoparticles (DMSNs)

DMSNs were synthesized following a literature procedure with minor modifications [29]. Briefly, cetyltrimethylammonium bromide (CTABr, 760 mg, 2.09 mmol) and sodium perfluorooctanoate (FC8, 160 mg, 0.35 mmol) were added to a solution of triethylamine (TEA, 136 mg, 1.04 mmol) in deionized water (50 mL) with stirring. The reaction mixture was stirred at 80 °C for 1 h. Tetraethyl orthosilicate (TEOS, 4.0 mL, 20.56 mmol) was added to the reaction mixture with vigorous stirring and stirred for 2 h. The obtained DMSNs were collected via centrifugation (10,000 g, 20 min) and washed 3 times with deionized water (20 mL) and dried at 60 °C overnight. Finally, synthesized DMSNs were gathered after calcination at 550 °C for 6h in air to remove the surfactant in and around the voids.

2.3.2. Synthesis ***S1***

DMSNs (100 mg) were dispersed in deionized water (4.0 mL) containing doxorubicin (Dox, 10 mg, 0.02 mmol, Carbosynth, Newbury, UK), and stirred for 24 h at room temperature. The dispersion was washed 3 times via centrifugation (10,000 g, 20 min) with deionized water (20 mL) to remove excess drug and the loaded nanoparticles (**S1**) were dried. The loading efficiency was calculated by the equation:

Percentage of loading = (total added Dox – non-loaded Dox)/total added Dox.

The quantity of non-loaded Dox was determined using a calibration graph based on measurements taken by spectrofluorometer at 480 nm/590 nm (excitation/emission).

2.3.3. Synthesis of ***S2***

S1 (50 mg) was suspended in PBS (41 × 2 mL) including PEI (25 mg, Mw = 25 kDa) and stirred for 4h at room temperature. Then, nanoparticles were centrifuged (10,000 g, 15 min) and resuspended in a DNase-RNase free water solution, obtaining as a result DMSN particles loaded with doxorubicin and covered by a layer of PEI (**S2**).

2.3.4. Synthesis of ***S3*** as control particles

Particles containing layers of PEI and PLL were prepared as controls. For that purpose, DMSN particles (50 mg) were suspended in PBS (41 × 2 mL) including PEI (25 mg, Mw = 25 kDa) and stirred for 4h at room temperature. Then, nanoparticles were centrifuged (10,000 g, 15 min) and resuspended in a DNase-RNase free water solution. In a second step, a PLL solution (300 μL, 1.0 mg/mL in 0.5 M NaCl) was added to DMSN-PEI suspension, maintaining the suspension 3 h at room temperature under stirring. The resulting product **S3** was recovered by centrifugation (10,000g, 15 min), washed three times with water (20 mL) with the aim to remove the excess PLL, and lyophilized.

S3 was used to perform stability assays of particles and also to simulate *in vivo* adsorption of proteins into particles. For stability tests, **S3** (2 mg) was dispersed in water, vortexed and incubated at room temperature for one week and then, hydrodynamic diameter was analyzed. On the other hand, to observe the possible protein adsorption into the particles, 2 mg of **S3** were dispersed in water and DMEM supplemented with 10 % FBS (1 mL). Then the mixtures were vortexed and incubated at 37 °C for 1 h, simulating *in vivo* circulating time [30] for plasma protein adsorption.

2.3.5. Synthesis of ***S4***

Particles containing layers of PEI, miRNA, PLL and no doxorrubicin were prepared as controls. For that purpose, DMSN particles (50 mg) were suspended in PBS (41x; 2mL) including PEI (25 mg, Mw = 25 kDa) and stirred for 4h at room temperature. Then, nanoparticles were centrifuged (10,000 g, 15 min) and resuspended in a DNase-RNase free water solution (50 mg in 2500 μL water). In a second step, miRNA-424-3p (2 nmol) was added to 500 μL of suspension containing 10 mg of particles, and were incubated for 40 min at room temperature. The resulting product was recovered by centrifugation (10,000 g, 15 min), washed three times with water (20 mL) to remove the excess of miRNA, and lyophilized.

2.3.6. Synthesis of ***S5***

S5 particles were prepared as **S4** with some modifications, with the aim to obtain control particles of DMSN loaded with doxorubicin and containing only PEI and PLL layers. For that purpose, **S2** particles (10 mg) were resuspended with 0.5 mL of water. Then, a PLL solution (300 μL, 1.0 mg/mL in 0.5 M NaCl) was added to the suspension and conserved for 3 h at room temperature under stirring. The resulting control particles containing only the layers of PEI and PLL (**S5**) was recovered by centrifugation (10,000g, 15 min), washed three times with water (20 mL) to remove the excess PLL, and lyophilized.

2.3.7. Synthesis of ***S6***

S2 (10 mg) was suspended in DNase-RNase free water (500 μL). Then, miRNA-424-3p (2 nmol) was added and incubated for 40 min at room temperature. The resulting product was recovered by centrifugation (10,000 g, 15 min), washed three times with water (20 mL) to remove the excess of miRNA, and lyophilized. In a second step, particles were resuspended with water (0.5 mL), and a PLL solution (300 μL, 1.0 mg/mL in 0.5 M NaCl) was added and conserved for 3 h at room temperature under stirring. The resulting product containing the loaded doxorubicin and the layers of PEI, miRNA-424-3p and PLL (**S6**) was recovered by centrifugation (10,000g, 15 min), washed three times with

water (20 mL) to remove the excess PLL, and lyophilized.

2.3.8. Synthesis of *S7*

Anti-Gal3 was covalently anchored to the surface of 10 mg of **S6** particles through the ester active method, by adding in a first instance EDC (0.2 M, 500 μL) and NHS (0.4 M, 500 μL) solutions in MES buffer to a suspension of 10 mg of **S6** in 0.5 mL of water, and incubated for an hour. In a second step, Galectin-3 antibody (0.1 mL, 1 mg/mL) was added and incubated for 2h. The resulting product ***S7*** was recovered by centrifugation (10,000 g, 15 min), washed three times with water (20 mL), and dried for further experiments.

2.3.9. Synthesis of *S8*

S8 was prepared to obtain fluorescent labeled **S4** particles with antiGal3 and Fluorescein Isothiocyanate (FITC). For that purpose, water suspensions of **S4** (1 mg/mL) were incubated with antiGal3 for covalent binding as explained in ***S7*** synthesis process. After washing step S4-antiGal3 were incubated with 20 μL of FITC solution (1 mg/mL) at room temperature during 2h. Particles were centrifuged and washed with water with water (1 mL) three times. FITC binding was assessed by examined the supernatants using a spectrofluorometer at 495 nm/519 nm (excitation/emission) before being utilized in cell culture experiments (data not shown).

2.4. In vitro Release behavior of the nanoparticles for Dox and miRNA-424-3p

To assess the release behavior of nanoparticles, PBS (pH 7.4) and lysosomal extract (pH 5.0, acquired from rabbit liver using an LYSISO1 kit in accordance with the instructions set out by the manufacturer) were used. In brief, rabbit livers were washed three times with cold PBS and homogenized in extraction buffer using an Ultra-Turrax. After serial centrifugation at 1000 and 20,000 g, the pellet was collected and separated by density gradient centrifugation at 150,000 g for 4 h. The integrity of the lysosomes in the collected lysosomal fractions was then assessed using the Neutral Red dye.

For this, 500 μg of nanoparticles were dispersed in 300 μL of PBS (pH 7.4) and lysosomal extract (pH 5.0) separately in four tubes and stirred at 37 °C. Then at each time interval, the tubes were centrifuged, and the supernatant fractions of the aliquots were measured to observe the release of Dox by obtaining fluorescence ($\lambda ex = 480$ nm, $\lambda em = 590$ nm) in a Jasco FP-8500 spectrofluorometer (Jasco Analitica, Spain) and of miRNA by Qubit™ 3 Fluorometer (Invitrogen™) following the manufacturer protocol (Qubit™ microRNA Assay Kits). For miRNA analysis, in brief, 10 μL of each sample was mixed with 190 μL of working solution in a tube and vortexed. Later, all the tubes were incubated at room temperature for 2 min and proceed to read standards and samples employing a Fluorometer.

2.5. Cell culture selection

A549 lung cancer cells were obtained from American Type Culture Collection (ATCC, Virginia). A549 were seeded in DMEM/High Glucose supplemented by 10 % (v/v) FBS and 1 % (v/v) penicillin-streptomycin (10,000 U/mL). Subsequently, the cells were maintained at 37 °C in an environment with 5 % CO_2.

2.6. Cell viability assay

A549 cells were seeded into 96-well plates to obtain a density of 5×10^3 cells in each well. After 24 h, the cells were treated with different nanoparticle formulations (**S3**, **S4, S5,** and **S6**) at different concentrations (200, 100, 50, 25, 10, 5, 1, 0.5, and 0.1 μg/mL), as well as, untreated cells as controls. Cell viability was analyzed after 24h of the nanoparticle treatments, by using WST-1 cell viability assay (Roche Diagnostics, Mannheim, Germany) following the manufacturer's protocol. After 2 h of incubation with WST-1 reagent, the occurred color development was measured with a test wavelength of 450 nm in VICTOR X5 PerkinElmer (ELISA plate reader).

2.7. Cell transfection

To transfect the cells with nanoparticles, forward transfection method was applied. For this A549 lung cancer cells were seeded in a 6-well plate 24h before transfection. Then, cells were transfected with nanoparticles loaded with miRNA-424-3p (**S4, S6,** and **S7**). Positive control cells were transfected with miRNA-424-3p alone and Lipofectamine® RNAiMAX Transfection Reagent plus miRNA-424-3p (Lipo + miRNA), which was used following the manufacturer's instructions. This reagent is a RNAi-specific cationic lipid formulation that facilitates the formation of lipid-RNA complexes enhancing delivery of miRNA and used as a control group. Accordingly, nanoparticles and other reagents were diluted in Opti-MEM® Reduced Serum Medium. For a 6-well plate each DMSN containing at least a quantity of 25 pmol of miRNA was added. After 4h incubation fresh cell medium was added and treatment was prolonged for 24h. Then cells were collected via centrifugation and used for further analysis.

2.8. Apoptosis analysis

To evaluate the apoptosis effect of nanoparticles loaded with and without miRNA on lung cancer cells, cells were seeded in 6-well plates at 2×10^5 cells per well. After 24 h, the cells were treated with different formulations of nanoparticles (50 μg/mL) and incubated for 24 h. Then, the cells were gathered and stained with annexin V-FITC and PI in annexin V binding buffer with CoraLite® Plus 488-Annexin V and PI Apoptosis Kit (Proteintech, Germany) in accordance with the manufacturer's protocol. The spectrum was collected for Annexin V (488/515 nm) and for PI (535/617 nm). Briefly, after treatment, the cells were collected, centrifuged and the cell pellet was resuspended in 400 μL of binding buffer (including 2 mL of 100 mM Hepes, 164 mg NaCl, 5.5 mg $CaCl_2$ and 18 mL of ddH_2O, pH 7.4). The cells were then stained with 5 μL of CL-488 Annexin V and 5 μL of PI working solution and incubated for 15 min in the dark at room temperature. The cells were sorted out using CytoFLEX S (Beckman-Coulter, CA, USA) flow cytometer.

2.9. RT-PCR analysis

Total RNA was extracted from cells seeded at 2.0×10^4 cells/2 mL medium in 6-well plates, grown overnight, and transfected with different formulations of nanoparticles together with positive control for 24 h. The total RNA isolation procedure was performed using QIAzol ® Lysis Reagent and Qiagen miRNeasy Mini Kit according to the manufacturer's protocol. For analysis of target gene (Gal3) mRNA expression, RNA was reverse transcribed into cDNA using a reverse transcription kit (TaKaRa PrimeScript™ RT reagent Kit, Japan) powered by PrimeScript Reverse Transcriptase (PrimeScript RT) in duplicate reactions following the manufacturer's instructions and using recommended PCR cycling conditions (reverse transcription: 37 °C, 15 min; inactivation of reverse transcriptase with heat treatment: 85 °C, 5 s).

The quantitative polymerase chain reaction (qPCR) was conducted on the LightCycler® 480 Instrument II Instrument (Roche) using the NZYSpeedy qPCR Green Master Mix Kit (NZYTech, Portugal). Each of the qPCR reaction mixtures included 2x NZYSpeedy qPCR Green Master Mix (2.5 μL); GADPH forward and reverse primers (0.5 μL, 10 μM); and a cDNA solution (2 μL) from reverse transcription, with nuclease-free water added to achieve a final volume of 10 μL. The thermal profile of the qPCR reaction was as follows: an initial denaturation step at 95 °C for 2 min, followed by 40 cycles of denaturation at 95 °C for 5 s, annealing/extension at 60 °C for 30 s, and fluorescence measurement at the endpoint. The expression levels of the different groups were evaluated in terms of their relative values compared with those of the control

group, which did not undergo transfection. The comparative threshold cycle ($2^{-\Delta\Delta Ct}$) was employed to determine this relative expression level. The reference gene, chosen for normalization, was Glyceraldehyde 3-phosphate dehydrogenase (GADPH) housekeeping gene. The following commercial LGALS3 primers were collected from Integrated DNA Technologies (IDT, Assay name Hs. PT.58.38902480, PrimeTime qPCR primers) used for Galectin-3: 5′-TTG TGC CTT ATA ACC TGC CTT-3′ (forward), 5′-TGG GTT AAA GTG GAA GGC AA-3′ (reverse). Each sample was prepared in triplicate and the fluorescence of each sample was analyzed in duplicate.

2.10. ELISA assays

For the assay, cells were seeded at a density of 2×10^5 cells per well in 6-well plates and allowed to grow overnight. The following day, the cells were treated with different formulations of nanoparticles for 24 h. Total protein extraction and ELISA assay were conducted using lysis buffer, which included proteases inhibitor, and Human Galectin-3 ELISA® Kit (Proteintech, Germany), respectively. The concentrations of proteins in solutions were determined using Pierce™ BCA Protein Assay Kits, in accordance with the manufacturers' protocols. The absorbance of each well was measured using an ELISA plate reader at 450 nm (ELISA assay) or 570 nm (BCA assay). Galectin-3 amount in 1 μg of protein extract was calculated for each sample by multiplying the resultant value by the suitable sample dilution factor and interpolating the absorbance values of the blank control subtracted against the standard curve. Sample preparation was done in triplicate, and each sample's absorbance was measured twice.

2.11. Imaging (Cellular uptake and lysosomal analysis)

To observe cellular uptake and lysosomal interaction during incubation, A549 cells on 24 mm diameter glass coverslips in 6-multiwell plates were incubated for 24 h to adhere. Then cells were treated with miRNA loaded and anti-Gal3 targeted DMSN for 6h. For confocal microscopy, coverslips were mounted, and prior to cell visualization, Hoechst 33342 (2 μg mL-1; Invitrogen, #H1399) and wheat germ agglutinin (WGA) Alexa Fluor 633 (1 μg mL^{-1}; Invitrogen, #W21404) were added for nuclei and membrane staining, respectively. In addition, to observe lysosomal analysis cells were also stained with Hoechst and LysoTracker Deep Red (Thermo Fisher Scientific Inc., cat. no. L12492) (0.1 μM for 30 min). After staining, cells were imaged with a Leica TCS SP8 high-speed confocal microscope equipped with a 405 nm laser, a 488 nm laser, a 552 nm laser, and a 638 nm laser using a 63× objective lens. The images were digitized and analyzed using Leica Application Suite X software.

2.12. SDS-PAGE

After treatment with different DMSN formulations, cells were collected to prepare a whole-cell lysate with a protease inhibitor mixture. Protein level (Gal3 and Endogenous GAPDH) measurement was performed using BCA assay. Protein extracts from the cells (30 μg of protein per well) were labeled with fluorescent dyes and then loaded, run on 10 % SDS-PAGE for 60 min at 150 V to separate the proteins. The Biorad ChemiDoc-XRS imaging system was used to visualize protein bands.

3. - Results and Discussion

3.1. Synthesis and characterization of nanoparticles

In this study, we have formulated a nanosystem based on a dendritic mesoporous silica nanoparticle (DMSN) containing doxorubicin (Dox) in the pores and capped by a layer-by-layer (LbL) of polyethyleneimine (PEI), miRNA-434-3p and poly-L-lysine (PLL). In addition, PLL was functionalized with an anti-Gal3 antibody (**S7**). The combination of chemotherapy and gene therapy represents a promising strategy in lung cancer treatment (see Scheme 2). First of all, DMSNs were obtained by an alkaline hydrolysis reaction involving tetraethylorthosilicate (TEOS), sodium hydroxide (NaOH), N-cetyltrimethylammonium bromide (CTAB), and perfluorooctanoic acid (FC8) [29]. This resulted in DMSNs (~110 nm) with a high pore size (~12 nm). In the synthesis, a fluorocarbon anion (FC8) was used to decrease the electrostatic interaction between the micelle and silicate, decreasing the surface tension of the CTAB micelle and improving the thermodynamic stability of the system to yield highly disperse and uniform DMSNs [29]. DMSNs were loaded with Dox (**S1**) by diffusion in a solution containing the nanoparticles and Dox. In a second step, the nanoparticles were capped by LbL functionalization with PEI as first layer (**S2**), miRNA-424-3p as second layer (DMSN-Dox-PEI-miRNA-424-3p) and PLL as third layer (**S4**). The attachment of PEI to the silanolate surface of DMSN primarily occurs through electrostatic interactions due to the positive charge of the amine groups present in PEI, which facilitates binding to the negatively charged silica surface. Then the negatively charged miRNA-424-3p was included as a second layer to **S2** through electrostatic interactions. Finally, the positively charged polymer PLL formed the external third layer (**S6**). In a final step, the anti-Gal3 antibody was covalently bonded to PLL chains via EDC/NHS chemistry [31] to give **S7**. In addition, control nanoparticles (**S3, S4** and **S5**) were synthesized by following the same procedure without the addition of Dox and/or miR-424-3p. It is expected that the blockage of the pores in **S7** would inhibit the release of the payloads before cell internalization ensuring miRNA and Dox delivery into the cytoplasm [32,33].

The successful preparation of nanocarriers was demonstrated using different characterization techniques including HRFESEM and TEM-EDX, DLS, FTIR, TGA, XRD, and BET. TEM and HRFESEM images showed that DMSNs were obtained as uniform nanospheres with an average particle size of 76 ± 7 nm (calculated with ImageJ software) with a dendritic central-radial pore structure (Fig. 1a and b). TEM-EDX mapping showed a chemical composition of Si: 37.5 ± 0.2, O: 55.8 ± 0.2, and C: 6.7 ± 0.3 (wt %), whereas no N was detected (Supporting Fig. S1). After LbL assembly, TEM-EDS mapping of **S3** indicated the presence of Si and O associated with the silica structure and an increase of C and N (Si: 27.2 ± 0.4, O: 23.8 ± 0.5, C: 57.9 ± 0.8, and N: 1.2 ± 0.9 (wt %) (Fig. 1c).

XRD studies were performed on DMSNs before and after calcination. The broad peak observed at 2θ 23° (Fig. 2a) collected at both spectra is assigned to the presence of amorphous silica of dendritic-MSN with a non-crystalline structure, in agreement with results reported in the literature [34].

The N_2 adsorption-desorption isotherms were used to determine the surface area, pore volume and pore diameter of the DMSNs by Brunauer–Emmett–Teller (BET) analysis. Studies on DMSN, **S3** and **S5** were carried out with the aim of observing the differences on the pore blockage. The nitrogen adsorption-desorption isotherm collected for DMSN is assigned to a type IV isotherm showing a capillary condensation-induced hysteresis cycle at relative pressures (P/P_0) in the range of 0.75–0.98, which indicated the nitrogen condensation inside the mesopores (Fig. 2b). The DMSN starting silica material has a specific surface area of 722 m^2/g, a pore volume of 0.7 cm^3/g and a pore diameter of 11.8 nm. In contrast, N_2 adsorption-desorption isotherms studies on **S3** allowed to calculate values of surface area of 201 m^2/g, pore volume of 0.6 cm^3/g and a pore diameter of 10.8 nm while it was 223 m^2/g, 0.3 cm^3/g and 9.6 nm for **S5,** respectively (Table 1). The high pore volume of DMSNs help to achieve a good encapsulation of both Dox and miRNA by optimizing different conditions (Supporting Fig. S4). A 90 % loading efficiency was obtained for Dox and 86 % for miRNA, measured by spectrofluorometer at 480 nm and Qubit™ Fluorometer at 498 nm, respectively.

The hydrodynamic diameter, particle size distributions and zeta potentials of the particles were studied by dynamic light scattering (DLS)

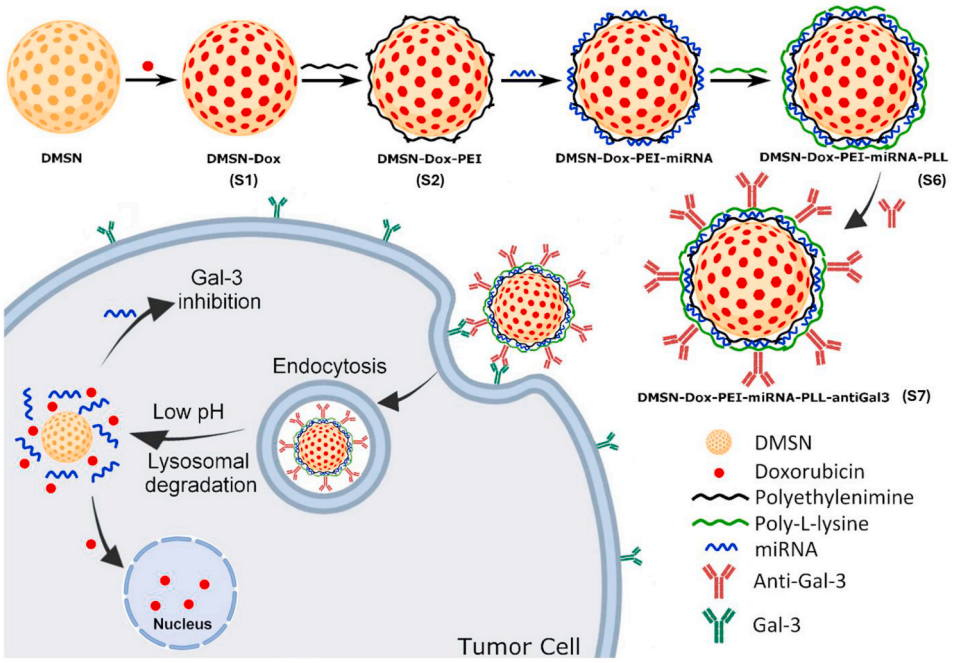

Scheme 2. Schematic illustration of the step-by-step preparation of layer-by-layer constructed dendritic mesoporous silica nanoparticles carrying Dox, microRNA 424-3p and anti-Gal3 (**S6**-*anti*-Gal3). The **S7** entered the cells via Gal3 receptor-mediated endocytosis. The acidic microenvironment allowed the release of Dox and microRNA 424-3p from the nanoparticles into the cytoplasm. Subsequently, Dox entered the nucleus, where microRNA 424-3p targeted the degradation of protein translation of Gal3, thereby inducing apoptosis.

(Fig. 2c and d). The hydrodynamic diameter of the starting DMSNs was 113 ± 5 nm and increased to 156 ± 5 nm after the Dox loading and PEI capping. The particle size of **S6** increased until 164 ± 7 nm with a narrow distribution of 0.26 ± 0.04 (polydispersity index), whereas the size of the final nanoparticle **S7** was 171 nm ± 4 nm. Regarding Zeta potential (ζ), it changed from −22.7 mV ± 1.4 of the starting DMSN nanoparticles to +28 mV ± 2.3 for **S6.** The incorporation of Gal3 to the final nanoparticle **S7** changed slightly the zeta potential to +31.5 ± 2.4 mV. In addition, FTIR and TGA studies of the different nanoparticle formulations were performed to monitor the successful synthesis of the nanoparticles (Supporting Figs. S2 and S3). Also, the nanoparticle **S3** was highly stable both in water and in DMEM with FBS (hydrodynamic diameter after 1 h: ca.140 nm, PDI: 0.406 in water and ca 139 nm, PDI: 0.443 in DMEM, respectively), suggesting no aggregation or protein corona formation after 1 h. Even after a week of incubation at room temperature, the nanoparticles dispersed in water showed high stability with no significant variation in hydrodynamic diameter. This agrees with previous studies using MSNs that found these nanoparticles remain stable in aqueous suspension for several weeks without significant aggregation or changes in hydrodynamic diameter [35,36].

3.2. The pH-sensitive release of Dox and miRNA

S7 is designed for the dual Dox and miR-424-3p, delivery and aims to achieve a synergistic effect on cancer cells. The stimulus-responsive release system was primarily designed to exploit the acidic environment of endosomes and lysosomes within tumor cells. Upon endocytosis, the PEI layer on the nanoparticles becomes protonated in the acidic endo/lysosomal compartments, leading to the "proton sponge" effect, endosomal rupture, and subsequent release of the loaded miRNA and Dox into the cytosol. This design ensures efficient intracellular delivery and release specifically in cancer cells. In our study release of Dox and miRNA from selected nanoparticles was tested in PBS and in lysosomal extracts. **S1** nanoparticles showed a high Dox release in 3 h in both PBS (>75 %) and lysosomal extract (>90 %), as expected due to the absence of gatekeeper (Fig. 3a). In contrast, **S2** nanoparticles showed only a 20 % Dox release in PBS in comparison to the 90 % Dox release observed in the medium with lysosomal extract. Finally, **S6** that is capped with the three layers (PEI, miRNA, and PLL) showed a Dox release of less than 10 % after 24 h in PBS, whereas release was higher than 90 % in the lysosomal extract. This experiment shows that the layer-by-layer coating on DMSN acts as an effective gatekeeper at neutral pH inhibiting Dox release. Payload delivery at acidic media (lysosomal extract) is attributed to the protonation of both PEI and PLL polymers that induces their detachment from the nanoparticle surface, opening the pores, and releasing Dox.

The release of miRNA in PBS and lysosomal extract from **S6** was also investigated. To perform this, Qubit™ microRNA Assay Kit was used which offers a fluorescence-based detection following the manufacturer protocol. Fig. 3b shows an insignificant release of miRNA (ca. 1 %) in PBS, in contrast to the lysosomal extract medium, where a significant amount of the miRNA (ca. 50 %) was released after 3 h, demonstrating that PLL detachment promotes miRNA release [30].

3.3. Biological function assays in delivering functional miRNA to cells

To further investigate if the designed DMSNs are effective carriers to deliver miRNA into the cytoplasm, confocal laser scanning microscopy (CLSM) live cell imaging was performed after treatment with **S8** (25 μg/mL), which was prepared from **S7** and labeled with FITC (green). Cells were monitored after treatment with the nanoparticles (Fig. 3c). Nanoparticles are mainly internalized by endocytosis, involving the formation of vesicles able to fuse with endosomes that are finally transferred into lysosomes. The intracellular fluorescence (in green) confirms the proper cellular uptake of the nanoparticles in A549 lung cancer cells. Considering that to achieve an efficient miRNA delivery, the nanoparticles must escape from the endosomes and reach the cytosol. A549 cells were stained with red fluorescent endosome/lysosome probe Lyso-Tracker DeepRed and then monitored after 24h incubation (Fig. 3c). After 30 min of treatment with the nanoparticles, an intracellular green fluorescent signal (associated with FITC) was observed and no overlapping signals between lysosomes (in red) and

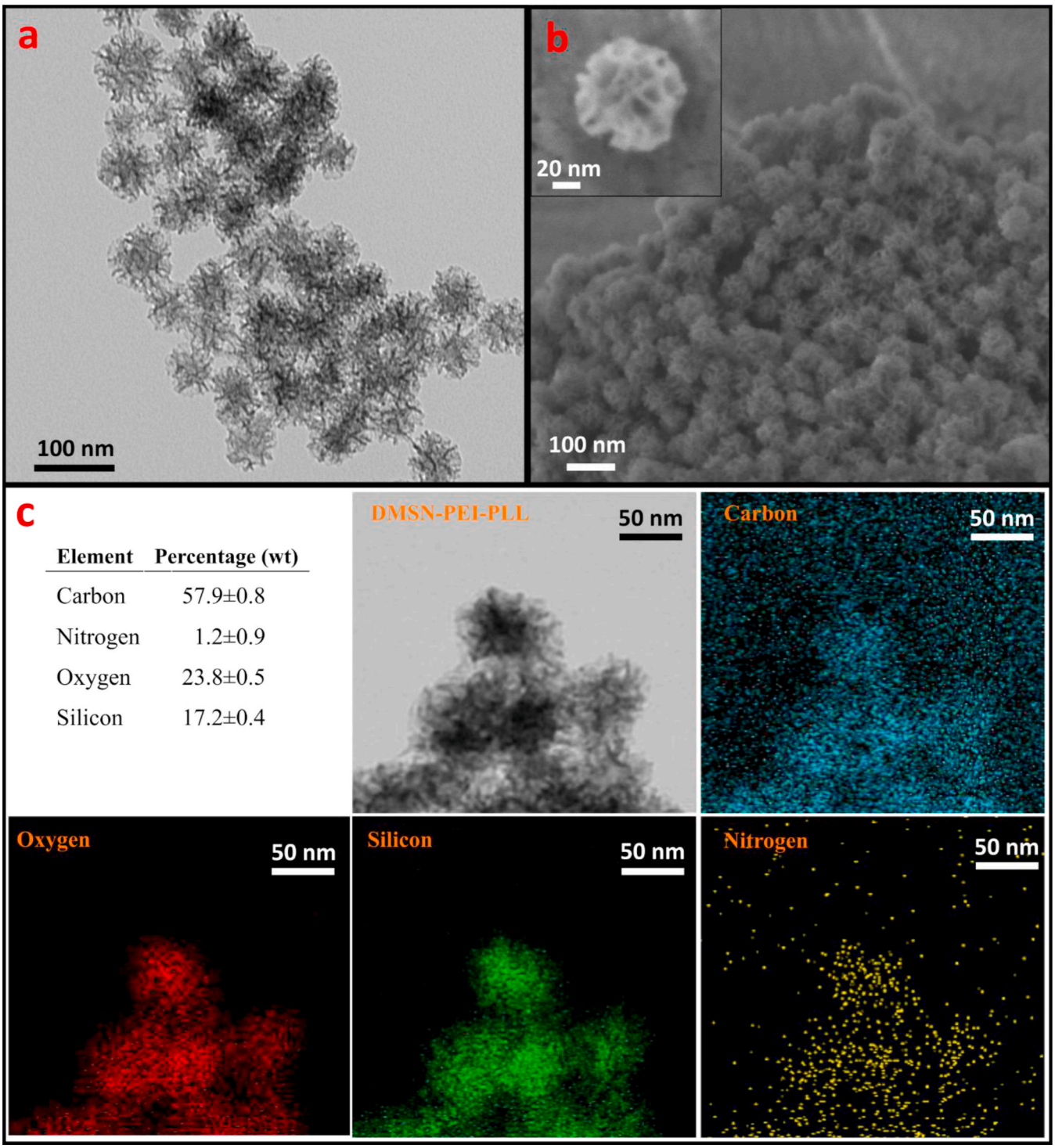

Fig. 1. Characterization of DMSNs. Analysis of the morphology of DMSNs by a) transmission electron microscopy (TEM) and b) high-resolution field emission scanning electron microscope (HRFESEM) and c) TEM-EDX elemental mapping of Si, O, C, and N of **S3.**

nanoparticles were detected. The results confirmed the proper uptake of the nanoparticles by lung cancer cells and stimuli-responsive cargo release, PEI-mediated endosomal escape due to protonation at acidic pH, resulting in endosome breakdown, and miRNA delivery into the cytosol. Similar results were reported by Meng et al. using a mesoporous dual Dox and Pgp siRNA delivery system coated with PEI that displayed effective cellular uptake [37–39].

Moreover, we also assessed that the delivery of the miRNA by **S7** in A549 cells downregulate the levels of Gal3. Bieg et al. hypothesized that miRNA-424-3p suppresses Gal3 in cancer cells either by suppressing the target gene or inhibiting protein synthesis [23]. There are two main mechanisms by which miRNAs silence genes: mRNA degradation and translation repression [40]. With the aim to evaluate the silencing efficiency of DMSN with different formulations on the mRNA level, RT-PCR was used in *vitro* gene silencing assays. The analysis was performed on RNA extracts obtained from A549 lung cancer cells to explore the effect of miR-424-3p on Gal3 expression (Fig. 3d). Following forward transfection, Gal3 expression in each group did not differ significantly

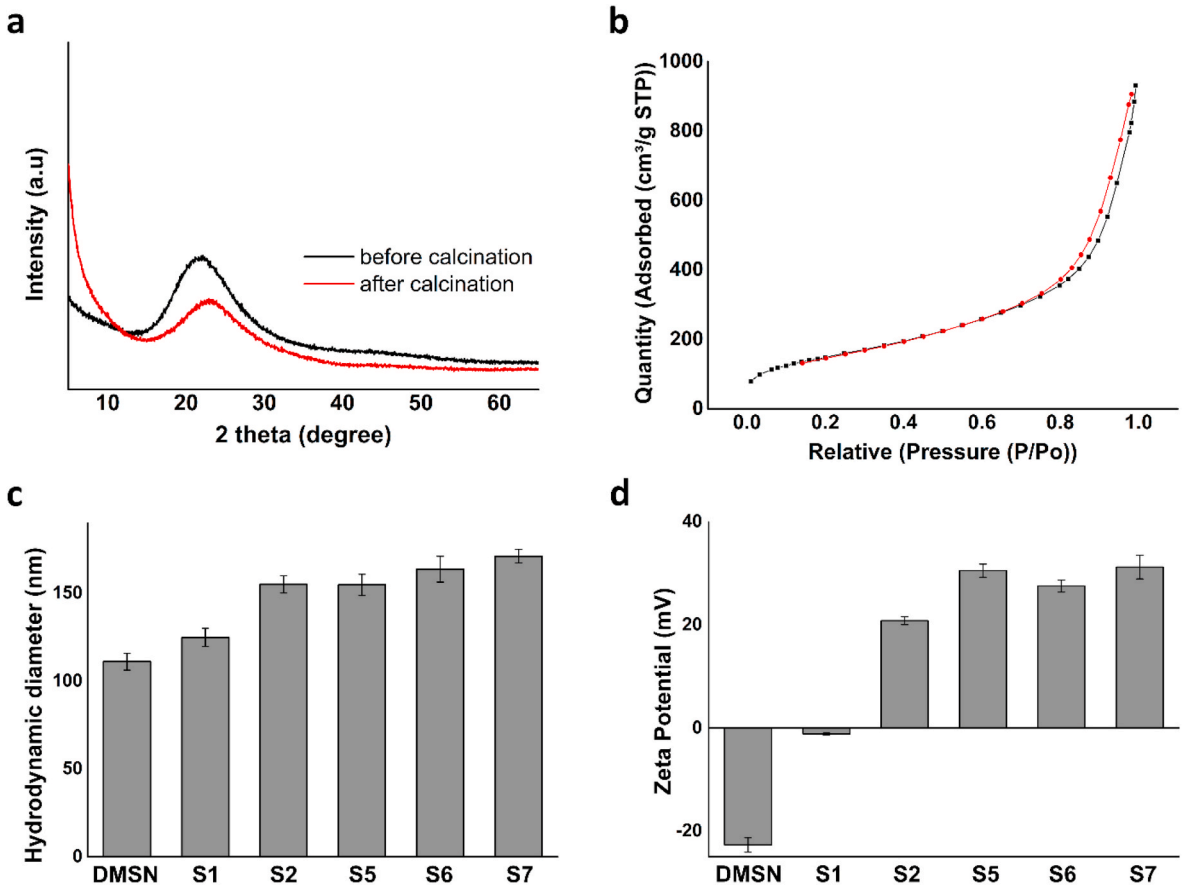

Fig. 2. a) High angle X-ray diffraction pattern of DMSNs before (black) and after (red) calcination, b) Nitrogen adsorption−desorption isotherms of DMSNs, c) Hydrodynamic diameter, and d) zeta potential of nanoparticles with different layers obtained via DLS measurements of materials **S1**-**S7**. (For interpretation of the references to color in this figure legend, the reader is referred to the Web version of this article.)

Table 1
Textural parameters of DMSN before and after modification obtained by nitrogen adsorption–desorption analysis.

Material	S_{BET} (m^2/g)	V_p (cm^3/g)	D_p (nm)
DMSN	722	0.7	11.8
S2	201	0.6	10.8
S5	223	0.3	9.6

compared to each relevant control. Considering the possible mechanism of miR-424-3p by inhibiting Gal3 translation without degrading the mRNA, we evaluate the effect at the protein level by ELISA analysis and SDS-Page [41]. As expected, the control group (cells without treatment) exhibited a high level of Gal3 protein in A549 lung cancer cells, thus confirming the suitability of the nanocarrier to deliver functional miRNA into cells for gene therapeutic applications [42,43]. After cell transfection with nanoparticles; **S4, S6**, and **S7,** the protein level decreased, which demonstrated that miRNA 424-3p carrying DMSNs suppressed the expression of Gal3 at the protein level and miRNA-424-3p regulates negatively Gal3 through direct targeting LGALS3 [44]. However, experiments with transfected cells with miRNA without any carrier system (free miRNA) or miRNA with Lipofectamine® RNAiMAX (Lipo + miRNA), showed a poor decrease in the protein level, which demonstrated that the developed nanocarrier is working efficiently (Fig. 3e). The effect of the combination of Dox and miRNA loaded DMSNs on the expression of Gal3 protein was assessed. A similar trend was observed by SDS-PAGE (Fig. S5 Supporting Information) confirming the efficient downregulation of Gal3 by the different formulations of nanoparticles, including miRNA-424-3p, suggesting that functionalized DMSNs were able to inhibit the expression of Gal3 protein in A549 cells. In contrast, DMSNs without miRNA (**S3**) and other control formulations (medium, Lipo + miRNA, and free miRNA) were not able to downregulate the protein in A549 cells. Overall, the data showed that the miR-424-3p with a suitable carrier reduced Gal3 expression (by approximately 50 % in the A549 cell line) at the protein level, with no effect on the mRNA level. Similar results were also obtained by Bieg et al. in which miR-424-3p decreased the expression of Gal3 in SK-OV-3 and TOV-21G cells at the protein level without degrading the mRNA [23]. Ramasamy et al. obtained that miR-424-3p reduced both mRNA and protein levels of Gal3 in BT549 breast cancer cells [24].

3.4. Cytotoxicity of DMSNs towards cancer cells

After the efficacy of designed DMSNs was confirmed to deliver the miRNA and to downregulate Gal3, its cytotoxic activity towards cancer cells was measured using the WST-1 assay (Fig. 4a). For this, A549 lung cancer cells were exposed for 24h to different concentrations of different nanoparticles ranging from 0.1 to 200 μg/mL. These studies were carried out with **S3**, **S4, S5** and **S6.** The cytotoxicity experiments demonstrated that **S3** has low toxicity on cells after 24h. The grade of cell survival in the presence of different amounts of **S3**, was between 99 ± 2 % (0.1 μg/mL) and 74 ± 5 % (200 μg/mL). Therefore, **S3** have minimal cytotoxicity and good biocompatibility, being therefore suitable for drug delivery. Then we tested the cytotoxicity of miRNA- and Dox-loaded DMSNs (i.e. **S5, S4,** and **S6**) in the same cell line. **S4** showed a cell survival at the 200 μg/mL concentration of 67 ± 4 % after 24h, and **S5** showed cell survival of 57 ± 4 %. The final system **S6** displayed the

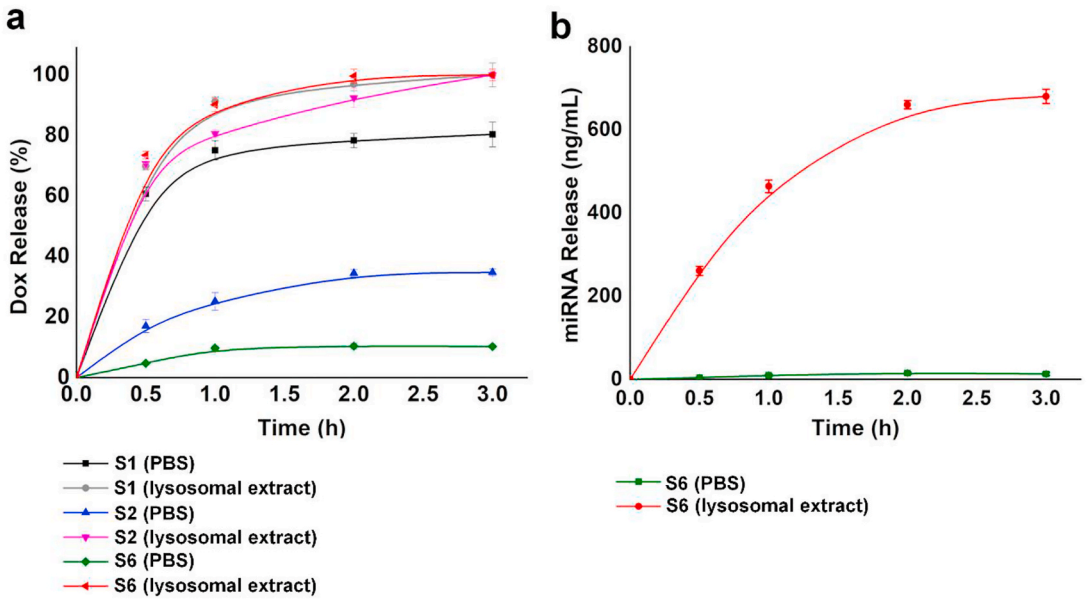

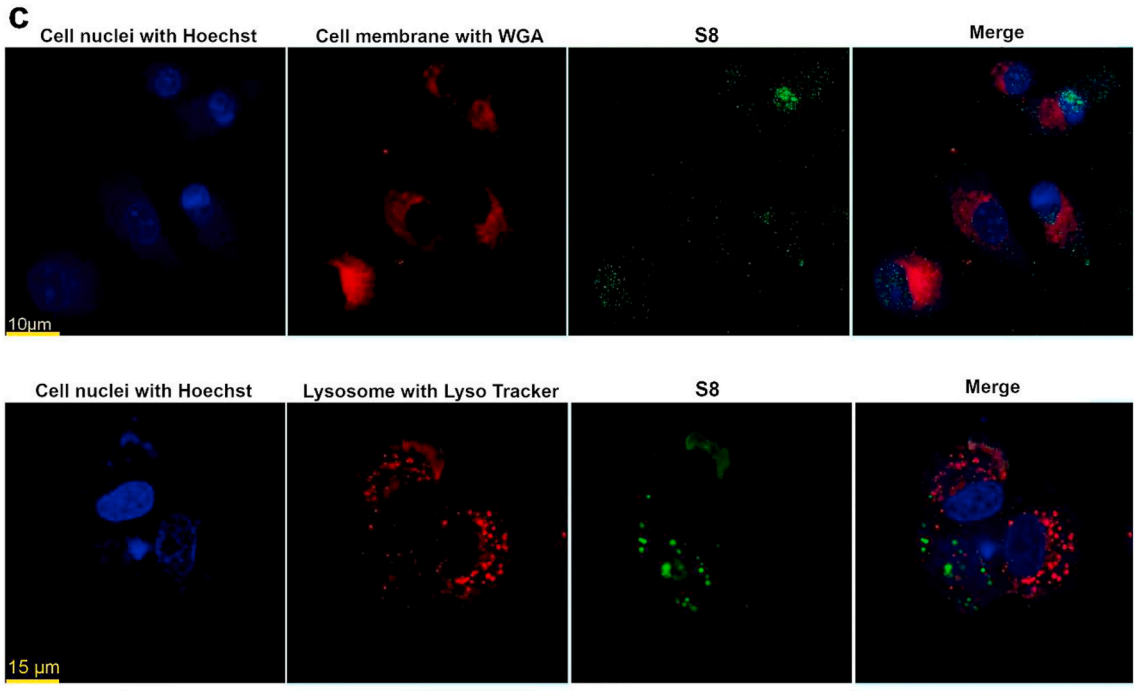

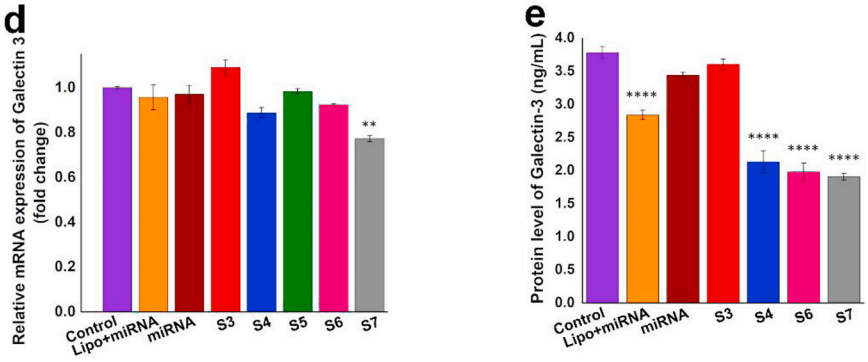

(caption on next page)

Fig. 3. Evaluation of the cargo release. a) *In-vitro* release of Dox in PBS and lysosomal extract determined by fluorescence measurements at different times (excitation/emission (ex/em)):470/495 nm), and b) miRNA in the absence or presence of lysosomal extract and PBS, acquired by measuring fluorescence at various times by a Qubit fluorometer at ex/em:498/518 nm. c) Cellular uptake of A549 cells by CLSM assay after 30 min incubation in A549 cells with **S8** nanoparticles. Cell nuclei were stained with Hoechst (blue), nanoparticles with FITC (green), cell membrane with WGA (red), and lysosomes with Lyso-Tracker DeepRed (red) and d) Relative mRNA expression of Gal3 after treatment of A-549 lung cancer cells with different DMSN formulations (**S1**-**S7**). Protein level of Gal3 after transfection obtained via e) ELISA assay (Control: medium, Lipo + miRNA: lipofectamine RNAimax + miRNA 424-3p, miR: miRNA 424-3p. Data are expressed as the mean ± SEM of at least three independent experiments, and statistical significance was assessed by one-way ANOVA and Tukey post-test (**p < 0.01 and ****p < 0.0001). (For interpretation of the references to color in this figure legend, the reader is referred to the Web version of this article.)

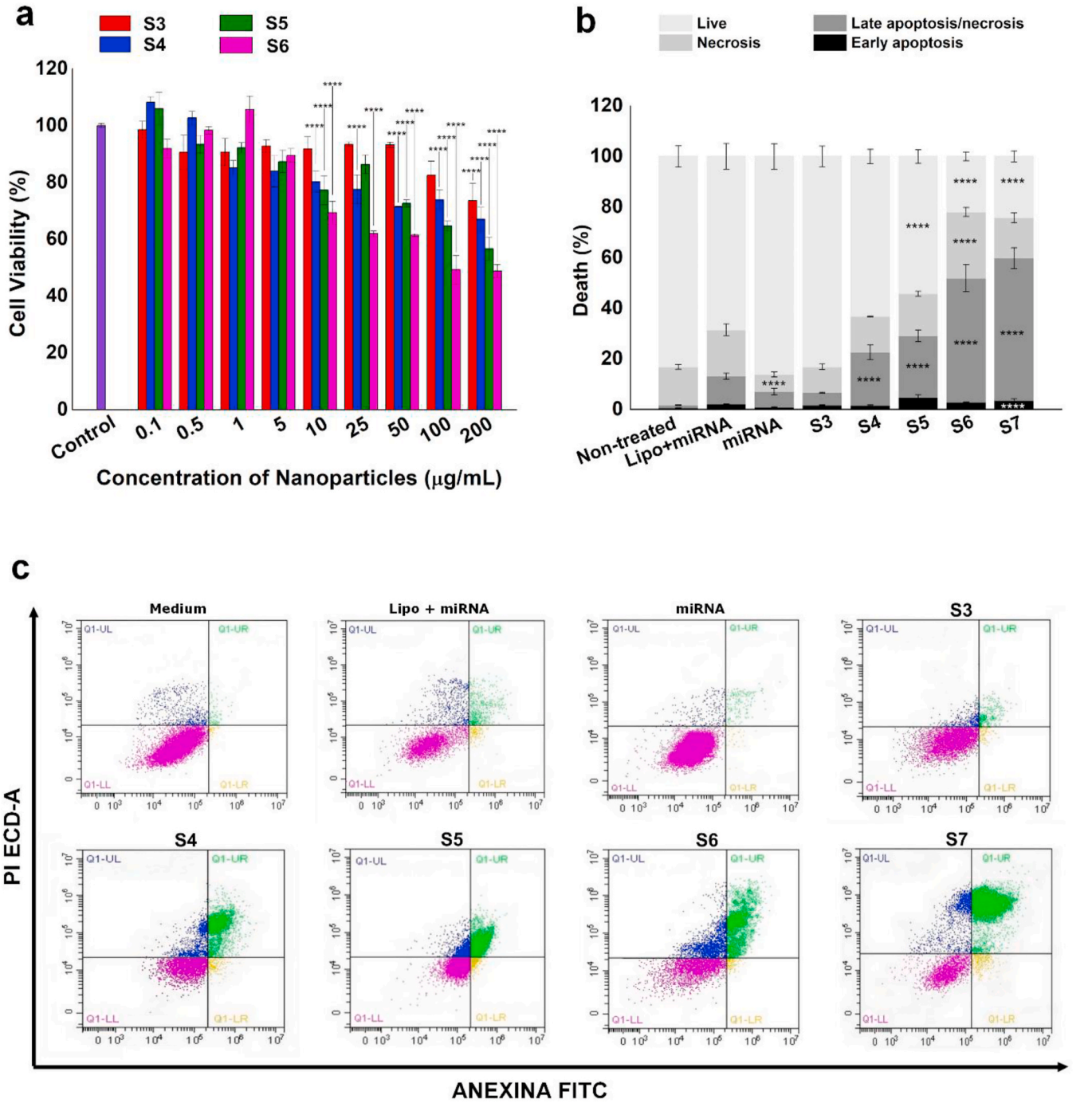

Fig. 4. a) Cell viability (%) of different formulations of DMSNs (**S3**- **S7**) analyzed with WST-1 assay for 24h, b) Quantification of early apoptotic, late apoptotic/necrotic, and necrotic cells, and c) Representative dot plot diagrams for apoptotic cell population was detected by flow cytometry (Annexin V/PI) after treatment of A-549 lung cancer cells with different DMSN formulations transfected with and without miRNA-424-3p. Percentages are expressed as the mean ± SEM of at least three independent experiments, and statistical significance was assessed by one-way ANOVA and Tukey post-test (****p < 0.0001).

lowest cell viability, with values of cell survival of 49 ± 2 % after 24h. The data indicates that the combination of miRNA and Dox in **S6** shows

the highest toxicity. Moreover, nanoparticle formulations containing both Dox and miRNA showed more toxicity than nanoparticles containing only Dox or miRNA. Our results are in line with Wang et al. who reported that miRNA-31 and Dox in MSN loaded with miRNA-31 and Dox with a PEI/hyaluronic acid coating, have a synergistic effect on mtEF4 cancer cells to induce cell death [45].

Finally, considering that Gal-3 is an anti-apoptotic protein highly expressed in A549 lung cancer cells [23], we aimed to investigate whether miR-424-3p delivered via DMSNs could downregulate Gal-3 and enhance the antitumoral effect of Dox by promoting apoptosis. To evaluate the therapeutic efficacy and elucidate the cell death mechanism of miRNA and Dox on A549 cells, apoptosis assays were performed using a double staining protocol based on AnnexinV/PI (Fig. 4b and c) measured via flow cytometry. The fluorescence intensity of the stained cells reflects the percentage of apoptosis, as both early and late apoptotic cells were positive for Annexin V-FITC staining. We compared nanoparticles carrying Dox and miRNA alone (**S4**/**S5**) with nanoparticles containing miRNA and Dox (**S6**) and also functionalized with anti-Gal3 (**S7**).

As expected, a higher apoptotic rate (late apoptosis-49 %) was achieved when the cells were treated with **S6** compared to that of **S5** (24 %) and **S4** (22 %), confirming the synergistic effect of Dox and miRNA co-delivery. Additionally, it was noted that the anti-Gal3 attached **S6** triggered a much higher apoptotic rate (late apoptosis/necrosis-56.27 %) than other groups. This enhanced effect can be attributed to multiple mechanisms: the anti-Gal3 antibody blocks the anti-apoptotic activity of Gal3, miR-424-3p downregulates Gal3 protein (and downstream Bcl2), and Dox accumulates in the nucleus to induce DNA damage. Additionally, the presence of anti-Gal3 may further enhance nanoparticle uptake via Gal3-mediated endocytosis, contributing to the observed increase in apoptosis. Untreated control cells (medium) and cells treated with empty nanoparticles (**S3**) showed low baseline cell death (~1–5 %), and the positive control (Lipofectamine + miRNA) exhibited only ~11 % late apoptosis/necrosis. Overall, this demonstrates that the DMSN-based formulation significantly improves the therapeutic effect of miRNA delivery, both by enhancing Gal3 downregulation and by combining it with Dox for synergistic apoptosis induction.

4. -Conclusion

In this study, we have successfully prepared dendritic mesoporous silica nanoparticles (DMSNs) loaded with Dox and capped with polyethyleneimine (PEI), miRNA-434-3p and poly-L-lysin (PLL) to combine the benefits of chemotherapy and gene therapy. It has been demonstrated that the co-delivery of miRNA-424-3p and Dox induce cell death by stimulating apoptosis and enhancing the efficiency on lung cancer treatment. *In-vitro* release profiles revealed that the acidic environment and lysosomal enzymes induced Dox and miRNA release from the **S6.** It was also shown that the miR-424-3p effectively transfected A549 lung cancer cells, significantly suppressing Gal3 expression at the protein but not at the mRNA level. Forward treatment of the cell line with **S7** induces the downregulation of Gal3 protein and together with Dox delivery, results in a significant reduction of cell viability. In the study, reduced oncoproteins (Gal3) expression via the co-delivery system led to increased apoptosis in A549 cells, more effectively than DMSNs individually loaded with miRNA-424-3p or Dox. These results demonstrated that the developed **S7** carrier system can be a good candidate for lung cancer treatment. Despite the growing attention toward combined strategies, such as the co-delivery of Dox and miRNAs, aimed at enhancing chemosensitivity and paving the way for future personalized cancer treatments, their clinical practice still faces challenges such as the stability and targeted delivery of miRNAs *in vivo*. Addressing challenges through innovations in nanoparticle design, such as stimuli-responsive systems, and thorough preclinical validation is essential to advance the clinical applicability of such strategies [46]. Furthermore, the therapeutic effects of miRNA-based interventions can vary significantly between patients due to tumor heterogeneity and differences in miRNA expression profiles. For example, while miRNA-424-3p is involved in critical oncogenic processes, its specific interaction with Galectin-3 in lung cancer is not well established [47]. Further research is still needed to elucidate the mechanism of miRNA-424-3p on Gal3 overexpressing tumor-bearing animal model which might provide a new idea for further investigation in lung cancer treatment. Overall, our findings point toward the potential of using layer-by-layer stimuli-responsive DMSNs as a promising approach for the systemic delivery of miRNAs in combination with drugs. These results encourage us to continue exploring their applicability in future studies.

CRediT authorship contribution statement

Oznur Akbal Vural: Writing – review & editing, Writing – original draft, Methodology, Investigation, Funding acquisition, Formal analysis, Conceptualization. **Tayfun Vural:** Writing – review & editing, Writing – original draft, Methodology, Investigation, Funding acquisition, Formal analysis, Conceptualization. **Vicente Martí-Centelles:** Writing – review & editing, Investigation. **Estela Climent:** Writing – review & editing, Supervision, Methodology, Investigation. **Alba García-Fernández:** Writing – review & editing, Methodology, Investigation. **Ramón Martínez-Máñez:** Writing – review & editing, Supervision, Methodology, Funding acquisition, Conceptualization.

Declaration of competing interest

The authors declare that they have no known competing financial interests or personal relationships that could have appeared to influence the work reported in this paper.

Acknowledgements

This research was supported by projects PID2021-126304OB-C41 and PID2024-155683OB-C41 funded by MICIU/AEI/10.13039/501100011033/and by European Regional Development Fund - A way of doing Europe. This study was also supported by Generalitat Valenciana (CIPROM/2021/007). We also acknowledge the Scientific and Technological Research Council of Turkey (TUBITAK 2219 Award # 1059B192201183) for Dr. Oznur Akbal Vural. V.M.-C. acknowledges the financial support from Project CIDEGENT/2020/031 funded by the Generalitat Valenciana, Project ESGENT/2024/001 funded by the Generalitat Valenciana, project PID2020-113256RA-I00 funded by MICIU/AEI/10.13039/501100011033, and Project CNS2023-144879 funded by MICIU/AEI/10.13039/501100011033 and European Union NextGenerationEU/PRTR. This research was supported by CIBER -Consorcio Centro de Investigación Biomédica en Red- (CB06/01/2012), Instituto de Salud Carlos III, Ministerio de Ciencia e Innovación. R.M.M. thanks to the European Union's Horizon EUROPE research and innovation programme under grant agreement No 101093042. E. C. thanks the Instituto de Salud Carlos III (Miguel Servet 2023 CP23/00086 and Project PI24_01239). O.A.V thanks Dr. Jennifer Soler for technical assistance on experimental design and all group members for their support.

Appendix A. Supplementary data

Supplementary data to this article can be found online at https://doi.org/10.1016/j.jddst.2026.107986.

Data availability

Data will be made available on request.

References

[1] J.P. Lima, L.V. dos Santos, E.C. Sasse, A.D. Sasse, Optimal duration of first-line chemotherapy for advanced non-small cell lung cancer: a systematic review with meta-analysis, Eur. J. Cancer 45 (2009) 601–607, https://doi.org/10.1016/j.ejca.2008.11.006.

[2] F.-M. Kong, R.K. Ten Haken, M.J. Schipper, M.A. Sullivan, M. Chen, C. Lopez, G. P. Kalemkerian, J.A. Hayman, High-dose radiation improved local tumor control and overall survival in patients with inoperable/unresectable non-small-cell lung cancer: long-term results of a radiation dose escalation study, Int. J. Radiat. Oncol. Biol. Phys. 63 (2005) 324–333, https://doi.org/10.1016/j.ijrobp.2005.02.010.

[3] N. Sawabata, E. Miyaoka, H. Asamura, Y. Nakanishi, K. Eguchi, M. Mori, H. Nomori, Y. Fujii, M. Okumura, K. Yokoi, Japanese lung cancer registry study of 11,663 surgical cases in 2004: demographic and prognosis changes over decade, J. Thorac. Oncol. : Official Publication of the International Association for the Study of Lung Cancer 6 (2011) 1229–1235, https://doi.org/10.1097/JTO.0b013e318219aae2.

[4] F. Sancenón, E. Yu, E. Aznar, M. Dolores Marcos, R. Martínez-Máñez, Gated porous materials for biomedical applications, Drug Deliv. Syst. (2017) 113–184, https://doi.org/10.1142/9789813201057_0004.

[5] A. Lérida-Viso, A. Estepa-Fernández, A. García-Fernández, V. Martí-Centelles, R. Martínez-Máñez, Biosafety of mesoporous silica nanoparticles; towards clinical translation, Adv. Drug Deliv. Rev. 201 (2023) 115049, https://doi.org/10.1016/j.addr.2023.115049.

[6] M. Ye, W. Zhang, H. Xu, P. Xie, L. Song, X. Sun, Y. Li, S. Wang, Q. Zhao, Fe-doped biodegradable dendritic mesoporous silica nanoparticles for starvation therapy and photothermal-enhanced Cascade catalysis in tumor therapy, J. Colloid Interface Sci. 678 (2025) 378–392, https://doi.org/10.1016/j.jcis.2024.08.172.

[7] Q. Zhao, S. Wang, Y. Yang, X. Li, D. Di, C. Zhang, T. Jiang, S. Wang, Hyaluronic acid and carbon dots-gated hollow mesoporous silica for redox and enzyme-triggered targeted drug delivery and bioimaging, Mater. Sci. Eng. C 78 (2017) 475–484, https://doi.org/10.1016/j.msec.2017.04.059.

[8] M. Wang, X. Li, Y. Ma, H. Gu, Endosomal escape kinetics of mesoporous silica-based system for efficient siRNA delivery, Int. J. Pharm. 448 (2013) 51–57, https://doi.org/10.1016/j.ijpharm.2013.03.022.

[9] X. Du, L. Xiong, S. Dai, F. Kleitz, S. Zhang Qiao, Intracellular microenvironment-responsive dendrimer-like mesoporous nanohybrids for traceable, effective, and safe gene delivery, Adv. Funct. Mater. 24 (2014) 7627–7637, https://doi.org/10.1002/adfm.201402408.

[10] S. Malekmohammadi, R.U.R. Mohammed, H. Samadian, A. Zarebkohan, A. García-Fernández, G.R. Kokil, F. Sharifi, J. Esmaeili, M. Bhia, M. Razavi, M. Bodaghi, T. Kumeria, R. Martínez-Máñez, Nonordered dendritic mesoporous silica nanoparticles as promising platforms for advanced methods of diagnosis and therapies, Mater. Today Chem. 26 (2022) 101144, https://doi.org/10.1016/j.mtchem.2022.101144.

[11] S.-N. Zhao, R.-H. Tang, S.-J. Deng, G.-E. Chen, J. Ye, Z.-L. Xu, Dual gatekeepers-modified dendritic mesoporous silica nanoparticles for controlled drug release, J. Mater. Sci. 58 (2023) 17610–17622, https://doi.org/10.1007/s10853-023-09128-5.

[12] C. Xu, M. Yu, O. Noonan, J. Zhang, H. Song, H. Zhang, C. Lei, Y. Niu, X. Huang, Y. Yang, C. Yu, Core-cone structured monodispersed mesoporous Silica nanoparticles with ultra-large cavity for protein delivery, Small 11 (2015) 5949–5955, https://doi.org/10.1002/smll.201501449.

[13] C. Deng, Y. Liu, F. Zhou, M. Wu, Q. Zhang, D. Yi, W. Yuan, Y. Wang, Engineering of dendritic mesoporous silica nanoparticles for efficient delivery of water-insoluble paclitaxel in cancer therapy, J. Colloid Interface Sci. 593 (2021) 424–433, https://doi.org/10.1016/j.jcis.2021.02.098.

[14] L. O'Driscoll, R. Linehan, Y.H. Liang, H. Joyce, I. Oglesby, M. Clynes, Galectin-3 expression alters adhesion, motility and invasion in a lung cell line (DLKP), in vitro, Anticancer Res. 22 (2002) 3117–3125.

[15] Y. Kataoka, T. Igarashi, Y. Ohshio, T. Fujita, J. Hanaoka, Predictive importance of galectin-3 for recurrence of non-small cell lung cancer, General Thoracic and Cardiovascular Surgery 67 (2019) 704–711, https://doi.org/10.1007/s11748-019-01074-x.

[16] P. Nangia-makker, V. Balan, A. Raz, Chapter 17 Galectin-3 binding and metastasis, in: Metastasis Research Protocols, Methods in Molecular Biology, 2012, pp. 251–266, https://doi.org/10.1007/978-1-61779-854-2.

[17] R. Buttery, H. Monaghan, D.M. Salter, T. Sethi, Galectin-3: differential expression between small-cell and non-small-cell lung cancer, Histopathology 44 (2004) 339–344, https://doi.org/10.1111/j.1365-2559.2004.01815.x.

[18] J.R. Sharma, A. Dubey, U.C.S. Yadav, Cigarette smoke-induced galectin-3 as a diagnostic biomarker and therapeutic target in lung tissue remodeling, Life Sci. 339 (2024) 122433, https://doi.org/10.1016/j.lfs.2024.122433.

[19] W.A. Chang, M.J. Tsai, P.L. Kuo, J.Y. Hung, Role of galectins in lung cancer, Oncol. Lett. 14 (2017) 5077–5084, https://doi.org/10.3892/ol.2017.6882 (Review).

[20] O.A. Kent, J.T. Mendell, A small piece in the cancer puzzle: microRNAs as tumor suppressors and oncogenes, Oncogene 25 (2006) 6188–6196, https://doi.org/10.1038/sj.onc.1209913.

[21] Y. Deng, C.C. Wang, K.W. Choy, Q. Du, J. Chen, Q. Wang, L. Li, T.K.H. Chung, T. Tang, Therapeutic potentials of gene silencing by RNA interference: principles, challenges, and new strategies, Gene 538 (2014) 217–227, https://doi.org/10.1016/j.gene.2013.12.019.

[22] Y. Wang, Y. Xie, K. V Kilchrist, J. Li, C.L. Duvall, D. Oupický, Endosomolytic and tumor-penetrating mesoporous silica nanoparticles for siRNA/miRNA combination cancer therapy, ACS Appl. Mater. Interfaces 12 (2020) 4308–4322, https://doi.org/10.1021/acsami.9b21214.

[23] D. Bieg, D. Sypniewski, E. Nowak, I. Bednarek, MiR-424-3p suppresses galectin-3 expression and sensitizes ovarian cancer cells to cisplatin, Arch. Gynecol. Obstet. 299 (2019) 1077–1087, https://doi.org/10.1007/s00404-018-4999-7.

[24] S. Ramasamy, S. Duraisamy, S. Barbashov, T. Kawano, S. Kharbanda, D. Kufe, The MUC1 and galectin-3 oncoproteins function in a microRNA-dependent regulatory loop, Mol. Cell 27 (2007) 992–1004, https://doi.org/10.1016/j.molcel.2007.07.031.

[25] M. Zhang, J. Zeng, Z. Zhao, Z. Liu, Loss of MiR-424-3p, not miR-424-5p, confers chemoresistance through targeting YAP1 in non-small cell lung cancer, Mol. Carcinog. 56 (2017) 821–832, https://doi.org/10.1002/mc.22536.

[26] Y. Hazeri, A. Samie, M. Ramezani, M. Alibolandi, E. Yaghoobi, S. Dehghani, R. Zolfaghari, F. Khatami, T. Zavvar, M.A. Nameghi, K. Abnous, S.M. Taghdisi, Dual-targeted delivery of doxorubicin by mesoporous silica nanoparticle coated with AS1411 aptamer and RGDK-R peptide to breast cancer in vitro and in vivo, J. Drug Deliv. Sci. Technol. 71 (2022) 103285, https://doi.org/10.1016/j.jddst.2022.103285.

[27] H. Yang, Y. Liu, Y. Qiu, M. Ding, Y. Zhang, MiRNA-204-5p and oxaliplatin-loaded silica nanoparticles for enhanced tumor suppression effect in CD44-overexpressed Colon adenocarcinoma, Int. J. Pharm. 566 (2019) 585–593, https://doi.org/10.1016/j.ijpharm.2019.06.020.

[28] X. Zhou, L. Chen, W. Nie, W. Wang, M. Qin, X. Mo, H. Wang, C. He, Dual-responsive mesoporous silica nanoparticles mediated codelivery of doxorubicin and Bcl-2 SiRNA for targeted treatment of breast cancer, J. Phys. Chem. C 120 (2016) 22375–22387, https://doi.org/10.1021/acs.jpcc.6b06759.

[29] Y. Wang, Y.A. Nor, H. Song, Y. Yang, C. Xu, M. Yu, C. Yu, Small-sized and large-pore dendritic mesoporous silica nanoparticles enhance antimicrobial enzyme delivery, J. Mater. Chem. B 4 (2016) 2646–2653, https://doi.org/10.1039/c6tb00053c.

[30] I. Garrido-Cano, A. Adam-Artigues, A. Lameirinhas, J.F. Blandez, V. Candela-Noguera, A. Lluch, B. Bermejo, F. Sancenón, J.M. Cejalvo, R. Martínez-Máñez, P. Eroles, Delivery of miR-200c-3p using tumor-targeted mesoporous silica nanoparticles for breast cancer therapy, ACS Appl. Mater. Interfaces 15 (2023) 38323–38334, https://doi.org/10.1021/acsami.3c07541.

[31] M. Biedulska, P. Jakóbczyk, M. Sosnowska, B. Dec, A. Muchlińska, A.J. Zaczek, D. Nidzworski, R. Bogdanowicz, Cytocompatibility of stabilized Black phosphorus nanosheets tailored by directly conjugated polymeric micelles for human breast cancer therapy, Sci. Rep. 11 (2021) 1–17, https://doi.org/10.1038/s41598-021-88791-7.

[32] T. Li, X. Shen, Y. Geng, Z. Chen, L. Li, S. Li, H. Yang, C. Wu, H. Zeng, Y. Liu, Folate-functionalized magnetic-mesoporous silica nanoparticles for Drug/Gene codelivery to potentiate the antitumor efficacy, ACS Appl. Mater. Interfaces 8 (2016) 13748–13758, https://doi.org/10.1021/acsami.6b02963.

[33] B. Gupta, H.B. Ruttala, B.K. Poudel, S. Pathak, S. Regmi, M. Gautam, K. Poudel, M. H. Sung, W. Ou, S.G. Jin, J.-H. Jeong, S.K. Ku, H.-G. Choi, C.S. Yong, J.O. Kim, Polyamino acid layer-by-layer (LbL) constructed silica-supported mesoporous titania nanocarriers for stimuli-responsive delivery of microRNA 708 and paclitaxel for combined chemotherapy, ACS Appl. Mater. Interfaces 10 (2018) 24392–24405, https://doi.org/10.1021/acsami.8b06642.

[34] H. Li, M. Zhang, J. Liu, J. Yang, X. Chen, M. Wang, H. Li, W. Zhu, Molybdenum-containing dendritic mesoporous silica spheres for fast oxidative desulfurization in fuel, Inorg. Chem. Front. 6 (2019) 451–458, https://doi.org/10.1039/c8qi00987b.

[35] A. Escudero, F.J. Hicke, E. Lucena-Sánchez, S. Pradana-López, J.J. Esteve-Moreno, V. Sanz-Álvarez, I. Garrido-Cano, S. Torres-Ruiz, J.M. Cejalvo, A. García-Fernández, P. Díez, R. Martínez-Máñez, Glucose-Fueled gated nanomotors: enhancing in vivo anticancer efficacy via deep drug penetration into tumors, ACS Nano 19 (2025) 20932–20955, https://doi.org/10.1021/acsnano.5c03799.

[36] A. García-Fernández, M. Sancho, E. Garrido, V. Bisbal, F. Sancenón, R. Martínez-Máñez, M. Orzáez, Targeted delivery of the pan-inflammasome inhibitor MM01 as an alternative approach to acute lung injury therapy, Adv. Healthcare Mater. 12 (2023), https://doi.org/10.1002/adhm.202301577.

[37] H. Meng, M. Liong, T. Xia, Z. Li, Z. Ji, J.I. Zink, A.E. Nel, Engineered design of mesoporous silica nanoparticles to deliver doxorubicin and P-glycoprotein siRNA to overcome drug resistance in a cancer cell line, ACS Nano 4 (2010) 4539–4550, https://doi.org/10.1021/nn100690m.

[38] X. Bai, Y. Huang, Y. Qin, Stimuli-responsive nano-carrier for Co-delivery of MiR-31 and doxorubicin to suppress high MtEF4 cancer, Applied Materials and Interfaces 10 (2018) 22767–22775, https://doi.org/10.1021/acsami.8b07698.

[39] P. Michael, Y.T. Lam, E.C. Filipe, R.P. Tan, A.H.P. Chan, B.S.L. Lee, N. Feng, J. Hung, T.R. Cox, M. Santos, S.G. Wise, Plasma polymerized nanoparticles effectively deliver dual siRNA and drug therapy in vivo, Sci. Rep. 10 (2020) 1–15, https://doi.org/10.1038/s41598-020-69591-x.

[40] Z. Li, R. Xu, N. Li, MicroRNAs from plants to animals, do they define a new messenger for communication? Nutr. Metabol. 15 (2018) 68, https://doi.org/10.1186/s12986-018-0305-8.

[41] Y.S. Lee, A. Dutta, MicroRNAs in cancer, Annual Review of Pathology 4 (2009) 199–227, https://doi.org/10.1146/annurev.pathol.4.110807.092222.

[42] L.-Y. Chung, S.-J. Tang, Y.-C. Wu, G.-H. Sun, H.-Y. Liu, K.-H. Sun, Galectin-3 augments tumor initiating property and tumorigenicity of lung cancer through interaction with β-catenin, Oncotarget 6 (2015) 4936–4952, https://doi.org/10.18632/oncotarget.3210.

[43] W. Zhou, X. Chen, Q. Hu, X. Chen, Y. Chen, L. Huang, Galectin-3 activates TLR4/NF-κB signaling to promote lung adenocarcinoma cell proliferation through activating lncRNA-NEAT1 expression, BMC Cancer 18 (2018) 580, https://doi.org/10.1186/s12885-018-4461-z.

[44] X. Chen, Y. Chen, Q. Hu, X. Chen, L. Huang, MiR-548c inhibits lung cancer cell proliferation through suppression of Galectin-3-mediated TLR4 signaling pathway, Int. J. Clin. Exp. Med. 11 (2018) 581–592.
[45] F. Wang, L. Zhang, X. Bai, X. Cao, X. Jiao, Y. Huang, Y. Li, Y. Qin, Y. Wen, Stimuli-responsive nanocarrier for Co-delivery of MiR-31 and doxorubicin to suppress high MtEF4 cancer, ACS Appl. Mater. Interfaces 10 (2018) 22767–22775, https://doi.org/10.1021/acsami.8b07698.
[46] S.W.L. Lee, C. Paoletti, M. Campisi, T. Osaki, G. Adriani, R.D. Kamm, C. Mattu, V. Chiono, MicroRNA delivery through nanoparticles, J. Contr. Release 313 (2019) 80–95, https://doi.org/10.1016/j.jconrel.2019.10.007.
[47] S. Li, Y. Wu, J. Zhang, H. Sun, X. Wang, Role of mirna-424 in cancers, OncoTargets Ther. 13 (2020) 9611–9622, https://doi.org/10.2147/OTT.S266541.